Precipitation in an Al-Mg-Cu alloy and the effect of a low amount of Ag

Mami Mihara[1,1*], Calin D. Marioara[2], Sigmund J. Andersen[2], Randi Holmestad[3], Equo Kobayashi[1] and Tatsuo Sato[4]

(Author's Affiliation)

1 Department of Metallurgy and Ceramics Science, Tokyo Institute of Technology, Tokyo 152-8552, Japan

2 SINTEF Materials and Chemistry, N-7465 Trondheim, Norway

3 Faculty of Physics, Norwegian University of Science and Technology, N-7491 Trondheim, Norway

4 Precision and Intelligence Laboratory, Tokyo Institute of Technology, Yokohama 226-8503, Japan (Present: Professor Emeritus)

1* Graduate student, Tokyo Institute of Technology

ABSTRACT

Two high-purity aluminium alloys based on composition Al-3.0Mg-1.0Cu (wt%), one with added 0.4 wt% Ag, were compared up to 11 days aging at 170 °C by means of hardness measurements and transmission electron microscopy. The base alloy exhibits an inhomogeneous precipitate microstructure with a high density of fine needle-shaped Guinier-Preston-Bagaryatsky (GPB) zones together with coarser precipitates of S'-Al_2CuMg and rods of the structurally unknown Z-phase. The S' phase is preferably formed on dislocations. The addition of Ag causes a strong effect, leading to a homogeneous precipitate microstructure with fine Ag-containing icosahedral quasi-crystalline precipitates (iQC). Both the GPB zones in the base alloy and the iQC phase in the Ag added alloy survive even after long term agin. Ag is found to suppress the formation of the S' phase. It is suggested that the iQC particles are structurally related to the Z phase as well as to the T-$Mg_{32}(Al, Cu, Ag)_{49}$ phase.

Keywords: aluminum-copper-magnesium alloy, precipitation, hardness, transmission electron microscopy (TEM), high-angle annular dark field scanning TEM, Guinier-Preston-Bagaryatsky (GPB) zones, S-phase, silver addition, micro-alloying

1. INTRODUCTION

Al-Cu-Mg alloys (2000 series alloys) are very important for aviation and automotive purposes. The highest strength is generally obtained with compositions producing a combined high density of fine S" and S' precipitates. The S" phase represents the Guinier-Preston-Bagaryatsky (GPB) zones, originally suggested by Bagaryatsky [1] to be a solute ordering structure formed on the {100} Al planes and by Silcock [2] to be "agglomerated one-dimentional (1D) crystals" along <100>Al directions - both descriptions can be said to be supported by recent studies in the atomic scale by high angle annual dark field scanning transmission electron microscopy (HAADF-STEM) and theoretical calculations [3-5]. S' is the representation of the stable S-phase in the Al matrix. The recent work reports that S and S' phases are structurally similar, with composition Al_2CuMg [6-7] and is the same structure as suggested originally by Perlitz and Westgren [8]. In the following, this phase will be referred to as S'.

Numerous publications exist concerning aging of the high strength Al-Cu-Mg alloys (see for example [9]). However, the medium strength Al-Mg-Cu alloys which are in focus here, are much less investigated although well suitable for commercially important applications such as body sheets for automobiles.. The high Mg/Cu ratio alloys lie in the α+S+T phase field of the equilibrium phase diagram. The age-hardening characteristics in the temperature range of 423-473 K is very similar to those of the lower Mg/Cu ratio alloys in the α+S phase field [10-11]. However, since the higher amount of Mg does not contribute to higher strength, commercialization of the alloys has been limited. According to classical studies [1-2] the precipitation of sequence is as follows; :

α (SSSS) → Cu/Mg nano-clusters → GPB zones (S”) → S’ → S (1)

SSSS refers to the super saturated solid solution in the Al (α) matrix and Cu/Mg nanoclusters are considered as precursors of the GPB zones. One of the characteristics of the aging behavior is that hardening mainly occurs in two distinct stages separated by a hardness *plateau*. The first increase is now believed to be attributed to solute clusters rather than to the formation of GPB zones [12]. Fine precipitation of GPB zones as well as the S'-phase is considered to cause the second stage of hardening. According to several previous studies on Al-Mg-Cu alloys containing industrial levels of Mn, Fe and Si, the T-phase has not been observed [13-14]. The T-phase is assumed to contain Cu instead of Zn however has same structure of the cubic T- $\boldsymbol{Mg_{32}(Al,Zn)_{49}}$ in Al-Zn-Mg alloys [15-16].

Small additions of particular alloying elements have been recognized to be effective in controlling Al-Mg-Cu alloy precipitate microstructure and properties [17-20]. According to several reports [20-22], silver is one of such elements with a tremendous influence on the age-hardening response. A micro-beam electron diffraction (MBED) study by Chopra et al. [23] indicated that the fine precipitates in the Al-1.5Cu-4.0Mg-0.5Ag (wt%) alloy are not isomorphous with the T phase. They proposed that the hardening precipitates in this alloy are the Z-phase. Hirosawa et al. [20] and Ringer et al. [21] also concluded that Ag enhances age-hardening by promoting precipitation of the Z-phase. It has been reported that the trace addition of Ag can promote theh formation of three different phases depending on the Cu:Mg ratio [23-25]. However, it is unclear that how impurity elements such as Mn, Fe and Si effect the results. Recently, Kubota et al. [26-27] reported that precipitates having a quasi-crystalline structure are the primary strengthening phase in the Al-10Mg-0.5Ag (wt%) alloy. The

quasi-crystalline phase in this alloy is structurally related to T- $Mg_{32}(Al,Ag)_{49}$ by similar internal atomic clusters (Bergmann clusters) [28-29]. In the present work we investigate two Al-Mg-Cu-(Ag) alloys. The alloys are prepared by high-purity materials in order to clarify the effects of the small addition of Ag on the age-hardening behavior and microstructures. .

2. EXPERIMENTAL

The chemical compositions of the alloys utilized in this work are listed in **Table 1**. Samples were solution treated in a salt bath at 793 K and kept for 3.6 ks, followed by quenching in ice-water and held for 60 s. The as-quenched condition is abbreviated 'A.Q.' in Fig. 1. The aging treatment was carried out in an oil bath at 443 Kfor various times.

Micro-Vickers hardness was measured with a load of 500 g for 15 s using a Mitsutoyo HM-102 micro-hardness tester. A value is based on a series of seven indentations. The maximum and minimum values were discarded and the average of the remaining five was used.

Specimens for transmission electron microscopy (TEM) were prepared by electro-polishing with a Tenupol 5 machine (Struers). The electrolyte consisted of 1/3 HNO_3 in methanol and the solution was kept at a temperature between 238 and 253 K. The precipitate microstructure was initially investigated by a conventional TEM in the bright-field mode using a Philips CM30 operated at 150 kV. The selected area (SA) diffraction patterns were from the interior of grains. Precipitate structures were investigated by high-resolution HAADF-STEM using a spherical aberration (C_s)

probe-corrected JEOL ARM 200F STEM operated at 200 kV. In order to reduce contamination all specimens were treated for a few minutes in a plasma cleaner (Fischinone 1020) before HAADF-STEM observations. To enhance contrast, high frequency noise of the HAADF-STEM images were removed by the fast Fourier transform (FFT) filtering using a circular band pass mask.

3. RESULTS AND DISCUSSION

3.1 Hardness evolution during aging at 443K

Fig. 1 shows the hardness results during aging at 443 K for the investigated alloys. In both alloys, a marked increase in hardness occurs in a short period during an initial stage then the hardness remains fairly constant for a long time, the plateau stage. The first stage is very short (in a few minutes) and contributes to improve hardness more than half of the total hardening in both alloys. The overall hardness of the Ag-added alloy is consistently higher than that of the Base alloy (a difference up to ~25 HV). Also, the plateau stage is shortened in the Ag-added alloy. The two alloys reach their maximum hardness after similar ageing time, 100 h. The addition of Ag somehow accelerates the precipitation kinetics of the base Al-Mg-Cu alloy, indicating the formation of a different and more effective hardening phase. In order to clarify the microstructure of precipitates TEM observation was performed.

3.2 Microstructure of precipitates

3.2.1 Precipitates in the Base alloy

Fig. 2shows TEM bright field images of the precipitates in the <001>Al orientation with corresponding SA diffraction patterns for the base alloy aged at 443 K for 10.8 ks, 86.4 ks, and for 950.4 ks, respectively. At the plateau stage no precipitates are directly detected , although weak spots are observed in the SA diffraction pattern demonstrating the existence of some precipitates as shown in Fig. 2(a). In a similar alloy, Kovarik [30] showed that the weak spots defining small squares between Al reflections including a central spot on the (forbidden) 110Al positions, as indicated with arrows in Figs. 2(a) and (b), are consistent with scattering from GPB/ GPB-II zones. For longer heat treatments the spots turn into the crosses as seen in Fig. 2(c), similarly centered, indicating the existence of the S' phase together with GPB zones (c.f. Ref. [31], Fig. 14). Thus, the microstructure at the end of this stage comprises rod-shaped Guinier-Preston-Bagaryatsky (GPB) zones and some S’ phase [Fig. 2(b)]. Also, the specimen at the peak hardness condition [Fig. 2(c)] exhibits a number of larger S’ phase particles heterogeneously nucleated on dislocations. Thus, as expected from the precipitation sequence (1) the S’ phase is predominantly formed in the Base alloy during ageing. The SA diffraction pattern in Fig. 2(c) together with HAADF-STEM images indicate that some fraction of GPB zones remains even after aging for 950.4 ks at 170 °C. What does not inconsistent with the precipitation sequence (1) is the presence of a cubic phase having relatively large square cross section [Fig. 2(c)] with diffraction patterns incompatible with both the S' and the T phases. It fits the structurally undetermined (fcc) phase Z which has a lattice constant very closed to the face diagonal of the T phase.

3.2.2 Precipitates in the Ag-added alloy

Fig. 3 shows TEM microstructures with SA diffraction patterns for the Ag-added alloy aged at 443 K for (a) 10.8 ks (b) 432 ks, and (c) 950.4 ks. From the BF images it is evident that the addition of Ag causes a drastic effect on the precipitate microstructure. In contrast with the base alloy, homogenious precipitates are observed even in the beginning of the age-hardening [Fig. 3(a)]. Although the contrast of the BF image of precipitates is different between two alloys, the selected area diffraction patterns in Fig. 2(a) and Fig. 3(a) are so similar.

Fig. 4 shows size distribution of the precipitate diameters in the Ag-added alloy aged for (a) 10.8 ks, (b) 432 ks, and (c) 950.4 ks. The precipitates follow a double distribution from the early stages, suggesting the existence of two types of precipitates. We interpret the smallest precipitates to be GPB/ GPB-II zones, which disappear gradually with ageing time in this alloy. At the peak hardness [Fig. 3(c)], the microstructure comprises a dense and homogeneous distribution of ~10 nm fine precipitates, while, as expected, the GPB zones are gone. A relatively small amount of coarser precipitates of the lath-shaped S' phase exist after prolonged aging, mainly associated with dislocations.

3.3 HAADF-STEM images of precipitates

3.3.1 Precipitates in the Base alloy

In the base alloy, three types of precipitates are observed after aging at 443 K for 950.4 ks [Fig. 2(c), (i)-(iii)]. First, nanoscale thin, needle-like particles extending along <001>Al are observed. These precipitates are GPB zones [Fig. 2(c), (i)]. The atomic

arrangement in the GPB zone structure is readily confirmed in the HAADF-STEM images. The zone cross-sections can be investigated in $<001>_{Al}$ orientation. The columns along <001>Al give rise to different intensities (I), which by the atomic number (Z) contrast with the intensity proportional to $Z^{1.7\text{-}1.9}$ [32-33]. A typical image of the cross-section of a GPB zone is given in Fig. 5. Individual columns are well resolved. The GPB zone and matrix have common (0.405 nm) periodicity in the viewing direction. A column is always associated with one of the two Al (001) planes of the 4.05 Å unit distance. The resultant element map in Fig. 5(b) shows that the lateral periodicity is missed, however, the structure is well defined in terms of units which are groups of 8 columns and stacked in various manners along <001>Al. The structure of these zones was first identified by Kovarik et al [3-5]. Based on their work we have chosen to label the center column as Al. even if the intensity of the center column varies and can approach the intensity of a Cu column due to an effect of the special Cu-rich environment.. This sets the formula of the group to $Al_2Mg_3Cu_3$. Also, some Al columns between the units have weaker contrast indicating some Mg incorporation. The GPB zones are often built by pairs of groups with the two partners of a pair having heights defined to neighbor Al (002) planes, combined in a way to give inversion symmetry (or a 2-fold screw axis parallel to the needle). There is a 1-1 correspondence with the Al columns and the positions and columns of height differing from Al concern the (Cu) group centers. The GPB zones are too small to be resolved in a conventional TEM Fig. 2, although their surrounding strain-fields are probably responsible for the grainy looking background of the BF images. However, they are exposed by their contribution of the weak spots to the SA diffraction patterns [31], as shown in Fig. 2(a) and discussed above.

Second, a class of larger precipitates in the base alloy, forming preferentially on dislocation lines [Fig. 2(c)-(ii)], was determined to be the S' phase [**Fig. 6 (a-c)**]. The Fig. 6 shows typical lath-like cross-sections with the particles extending all through the specimen. They are often found in groups with common a-axis along <001>Al, with the two other bases along mutually normal <120>Al directions [Fig. 6(b)], and with c-axis as the normal of the main lath-plane. Part of the interface of an S' lath is shown in Fig. 6(c), with unit cell and atomic overlay suggesting the interface column species. The main interface (trace along **b**$_{S'}$) is always coherent, since the buckled Al planes at Z=0, 1/2 (dotted lines) provide a good connection with the matrix.

In addition to particles of the S' phase, square cross sections appeared in Fig. 2(c)-(iii). The cross section belongs to a much coarser rod-like phase in the <001>Al orientation (**Fig. 7**). In the orientation along the rods we find a square cell and diffraction pattern which can fit two phases; T (a_T =14.16Å) [g] and Z (a_Z =19.99Å) [16] if indexed as a cubic structure, where $a_Z \approx a_T\sqrt{2}$. **Fig. 8** shows nano-beam electron diffraction (NBD) patterns (a) along and (b) perpendicular to the rods. Evaluating other zone axes, it was found that the patterns correspond with the Z phase as first reported by Chopra et al. [23] in an over-aged Al-1.5wt% Cu-4.0wt% Mg-0.5wt% Ag alloy aged for (100 days at 170 °C). Chopra et al [23] found two orientation relationships. It is clear that the particle in Figs. 7 and 8 follows the primary relationship, i.e. with parallel cube cells of Al and Z phase. The relation between the unit cells of Z phase and T phase indicates structural similarities, although it has been found that the phases must have different structures [23-24]. In the present experiments large particles of Z is found in the Base alloy only after the longest aging time. Although Z phase must also exist as small particles, the density suggests it is doubtful this phase contributes significantly to the

hardness of the base alloy. However, it has been also reported that trace additions of Ag will promote finely distributed precipitates of Z phase in Al-Cu-Mg ternary alloys [23-25].

3.3.2 Precipitates in the Ag-added alloy

In the Ag-added alloy, uniformly distributed fine precipitates were detected in the BF images from the shortest heat-treatment condition, see Fig. 3. This agrees with the previous observations [23-25], where Ag was found to promote the formation of the fine Z precipitates. The weak, squarely arranged spots in the SAD patterns in Fig. 3(b-c) match the ones between the Al reflection spots in the nano-beam diffraction pattern in Fig. 8(a). The squarely arranged spots divide the <001>Al zone pattern in five. This could in principle stem from an fcc structure with a lattice parameter about 2.025 nm, which differs from that of Z (a=1.999 nm [23]) by 1.3%. However, a detailed investigation showed that the weak spots were more likely to originate not from a single zone axis, but from precipitates oriented in the Al matrix with some high symmetry zone parallel with <110>Al directions. High resolution HAADF-STEM images of the precipitates indicated that they were disordered. However, images taken in <112> Al zones showed a 5-fold symmetry. An example is given in Fig. 9(a). This is corroborated by the FFT image from a part of the particle in a <112> Al zone, annotated by 'i'. It shows a ring of strong spots of near 5-fold intensity distribution [inset in Fig. 9(b)]. The weaker spots of the inner ring are less perfectly arranged. This may be a follow from (double) diffraction effects by the surrounding Al matrix. The contrast-improved inverse transformed image in Fig. 9(b) was overlaid by pentagons with vertices defined to the high intensity columns/positions. The pseudo-pentagonal

symmetry and lack of overall periodicity suggest the main precipitate in this alloy is an icosahedral quasi-crystal (iQC).

Al-5Mg and Al-10Mg alloys were investigated by Kubota [26-27] who showed that 0.5 wt% added Ag had profound effects on precipitation. In spite of the much higher Mg content in his alloys, the small, often spherical precipitate shape, distribution and the SA diffraction intensity visible in his patterns of the Ag-containing alloys have clear similarities with the present observations in the two longest heat-treatments. Thus, the Ag-containing precipitates are likely to be the similar icosahedral quasi-crystalline (iQC) particles. Kubota also demonstrated the similarity between the iQC particles and the T-$Mg_{32}(Al,Ag)_{49}$ phase both in diffraction and in composition [27]. He also found that the cube cells of α-Al and T to be parallel. Since T is an approximation phase to the iQC (related to the iQC of the Al-Mg-Zn system [26-29]), if composition and heat-treatment is not optimal it is likely that small regions of T could coexist with the iQC - and degrading symmetry, explaining the pseudo 5-fold pattern in Fig. 9(b).

The absence in the SAD of Fig. 3 of the crosses observed in the SAD in Fig. 2(c) shows the S' phase must be relatively sparse in the Ag-added alloy. S' particles were found to take the same orientation relationship as in the base alloy, but S' particles in Ag-added alloy have more roundish cross-sections. The amount was not quantified. One example of the S' particle in Ag-added alloy is given in Fig. 10. Compared with the base alloy (Fig. 6), it is obvious that the interface only occasionally coincides with a {120} Al plane, for example the upper and lower (more and less straight) interfaces with normal vectors along **c**. The lower right indicated plane with trace [120] Al has high contrast columns between the ones assigned to Cu (see Fig. 6 (b) ? where a

similar interface is indicated). The particle in Fig 10 has strong contrast columns at the boundary with intensity varying from place to place; the upper right part contains a darker region, whereas most of the left interface contains strong contrast columns breaking the normal period. It is likely, but still unclear how these effects are related to Ag. Dedicated experiments would be needed to determine where the Ag atoms are.

A question is why the Ag containing precipitates do not give rise to additional diffraction spots in the SAD patterns after aging for 10.8 ks [Fig. 3(a)]. Small size and roundish shape in combination with a disordered or quasi-crystalline structure will tend to spread the intensity, which would be part of the explanation. Additionally, Fig. 4 shows that the majority of the precipitates in this condition are on the order of one unit cell. This means that they are on the cluster-stage, presumably containing just one or a few of the Bergmann atomic clusters common for the T-phase and the iQC. Lack of periodicity will prevent normal diffraction spots. We suggest that this is the reason for the similarity of the diffraction spots in two alloys aged for 10.8 ks. These clusters are likely to be building blocks of the Z-phase as well. The unit cell of T-$Mg_{32}(Al,Zn)_{49}$ contains 162 atoms, in two Bergmann clusters, which can be viewed as constructed by several atomic shells [16, 29]. The structure of the Z- phase is not known. Z phase is not an isomorph of the T-phase [23] but still have close structural relation. The intensity distribution along the <111>Z direction suggests that the diffraction patterns in Fig. 8 bear the mark of icosahedral symmetry. For example the intensity is high for the first, third, and fifth spots. These are the Fibonacci indices, closely connected with the geometry of the icosahedron, with the icosahedral quasicrystals and with their approximation phases. It is therefore a strong indication that Z is an approximation phase for the iQC phase [34-35]. The larger size of the Z-phase could indicate that an

extra shell has been added to the Bergmann type cluster of the T-phase, as is not uncommon for approximation phases [34-35]. The formation mechanism of the Z phase and the structural correlation between the T phase and the Z phase remain to be fully understood.

5. CONCLUSIONS

(1) The Base alloy initially was hardened by a high density of GPB/ GPB-II zones . S' laths were predominantly formed on dislocations. Longer ageing led to combinations of GPB zones (which may be described as assemblies of $Mg_3Cu_3Al_2$ column groups along directions) and S' precipitates. A third phase consisting of large rods extending along , having square cross-sections were determined to be the cubic Z-phase, with cell

which the unit cell is parallel with Al. The GPB zones survived for long heat-treatment times.

(2) By the addition of 0.4 wt% Ag to an Al - 3 wt% Mg -1 wt% Cu alloy, the hardness was consistently higher with a peak hardness increase from ~ 92 HV to ~118 HV and the precipitate microstructure was much more homogeneous.

(3) In the Ag-added alloy, from the beginning of the heat-treatment the GPB/ GPB-II zones coexisted with a high density of Ag-containing precipitates. The pseudo-pentagonal symmetry and lack of overall periodicity suggested that the dense precipitates are icosahedral quasi-crystals. HAADF-STEM showed the isosahedral quasi-crystals tended to deviate from perfect symmetry, possibly because of an intermix with small regions of the cubic approximation phase T-Mg_{32}(Al, Cu, Ag)$_{49}$.

(4) The Z phase was not found in the Ag-added alloy. However, the diffraction patterns indicated that the structure of the Z-phase must be related to T-phase. It is suggested that Z-phase contain similar (Bergmann) atomic clusters, with one or more extra shell than in the T-phase or icosahedral phase. In the Ag added alloy the S' phase was found to be smaller, with a more roundish cross-section, and with extra Ag or Cu columns in the interface.

6. ACKNOWLEDGEMENTS

The authors are grateful to UACJ Corporation for material supply. Present authors appreciate to Tokyo Institute of Technology Academy for Co-creative Education of Environment and Energy Science and Japan Aluminium Association Research Grant Program for the financial support.

The Norwegian participants of this work (C. D. Marioara, S. J. Andersen and R.

Holmestad) acknowledge support from The Research Council of Norway, supported this project through the Frinatek FRINATEK project No: 221714. The TEM work was carried out on the NORTEM facility, TEM Gemini Centre, Norwegian University of Science and Technology (NTNU), Norway.

7. REFERENCES

[1] Y. A. Bagaryatsky, *Dokl. Akad. SSSR* **87** (1952) 397-401

[2] J. M. Silcock, *J. Inst. Met.* **89** (1960-61) 203-210

[3] L. Kovarik, S. A. Court, H. L. Fraser, M. J. Mills, *Acta Mater.* **56** (2008) 4804-4815

[4] L. Kovarik, M. J. Mills, *Scripta Mater.* **64** (2011) 999-1002

[5] L. Kovarik, M. J. Mills, *Acta Mater.* **60** (2012) 3861-3872

[6] B. Heying, R-D. Hoffmann, R. Pöttgen, Z. *Naturforsch.* **60B** (2005) 491-494

[7] Z. R. Liu, J. H. Chen, S. B. Wang, D. W. Yuan, M. J. Yin, C. L. Wu, *Acta Mater.* **59** (2011) 7396-7405

[8] H. Perlitz, A. Westgren, *Ark. Kemi, Mineral Geol.* **16B** (1943) 1-5

[9] J. Yan, PhD thesis: *Strength Modelling of Al-Cu-Mg Type Alloys*, March 2006, Univ. of Southampton, England, Faculty of Engineering, Science & Math.

[10] P. Ratchev, B. Verlinden, P. De Smet, P. Van Houtte, *Acta Mater*. **46** (1998) 3523-3533

[11] P. Ratchev, B. Verlinden, P. De Smet, P. Van Houtte, *Mater. Trans. JIM* **40** (1999) 34-41

[12] S.P. Ringer, Kazuhiro Hono, Toshio Sakurai and I.J. Polmear, *Scripta Materialia*, **36, No. 5** (1997) 517-521

[13] P. Ratchev, B. Verlinden, P. van Houtte, *Scripta Met. Mater*. **30** (1994) 599-604

[14] S. Hirosawa, T. Omura, Y. Suzuki, T. Sato, *J. Jpn. Inst. Light Metals* **56** (2006) 673-679

[15] J. H. Auld, J. T. Vietz, I. J. Polmear, *Nature* **209** (1966) 703-704

[16] G. Bergman, J. L. T. Waugh, L. Pauling, *Acta Cryst* **10** (1957) 254-259

[17] I. J. Polmear, S. P. Ringer, *J. Jpn. Inst. of Light Metals* **50** (2000) 633-642

[18] S. Hirosawa, T. Sato, *Metals* **73, No. 3** (2003) 191-195

[19] T. Sato, S. Hirosawa, K. Hirose, T. Maeguchi, *Metall. Mater. Trans.* **34A** (2003) 2745-2755

[20] S. Hirosawa, T. Omura, Y. Suzuki, T. Sato, *Mater. Sci. For.* **519-521** (2006) 215-220

[21] S. P. Ringer, G. C. Quan, T. Sakurai, *Mater. Sci. Eng. A* **250** (1998) 120-126

[22] C. Li, G. Sha, B. Gun, J. H. Xia, X. F. Liu, Y. Y. Wu, N. Birbilis, S. P. Ringer,

Scripta Mater. **68** (2013) 857-860

[23] H. D. Chopra, B. C. Muddle, I. J. Polmear, *Phil. Mag. Lett.* **73** (1996) 351-357

[24] H. D. Chopra, L. J. Liu, B. C. Muddle, I. J. Polmear, *Phil. Mag. Lett.* **71** (1995) 319-324

[25] I. J. Polmear: *Light Alloys*, 4th ed, Elsevier / Butterworth-Heinemann, Amsterdam (2006)

[26] M. Kubota, J. F. Nie, B. C. Muddle, *Mater. Trans. A* **46** (2005) 1278-1287

[27] M. Kubota, PhD thesis: *The precipitation hardening response in Al-Mg(-Ag) alloys*, Aug. 2001, Monash University, Dept. Mater. Eng., Clayton, Victoria 3168, Australia

[28] G. Bergman, J. L. T. Waugh, L. Pauling, *Acta Cryst.* **10** (1957) 254-259

[29] M. Audier, P. Guyot, *Extended Icosahedral Structures*, San Diego: Academic Press (1989).

[30] L. Kovarik, P.I. Gouma, C. Kisielowski, S.A. Court and M.J. Mills, *Acta Mater.* 52 (2004) 2509-2520.

[31] S. C. Wang, M. J. Starink, *Int. Mater. Rev.* **50** (2005) 193-215

[32] S. J. Pennycook, S. D. Berger, R. J. Culbertson, *J. Microsc.* **144** (1986) 229-249

[33] S. J. Pennycook, *Adv. Imag. Electr. Phys.* **123** (2002) 173-206

[34] K. Hiraga, T. Ohsuna, K. Sugiyama, *Rigaku Journal* **16** (1990) 38-45

[35] W. Steurer, *Z. Kristallogr.* **219** (2004) 391-446

[36] Ph. A. Dubey, B. Schönfield, G. Kostortz, *Acta Metall. Mater.* **39** (1991)1161-1170

[37] C. Li, C. Niu, Z. Du, C. Guo, Y. Jing, Calphad: *Computer Coupling of Phase Diagrams and Thermochemistry* **34** (2010) 120-128

[38] R. Baur, V. Gerold, *Acta Metall.* **10** (1962) 637-645

Table 1 Chemical compositions of the currently investigated alloys in wt%.

Alloy/ Element (wt%)	Mg	Cu	Ag	Si	Fe	Al
Base alloy	3.04	1.01	-	0.01	0.01	Bal.
Ag-added alloy	3.05	0.99	0.41	0.00	0.00	Bal.

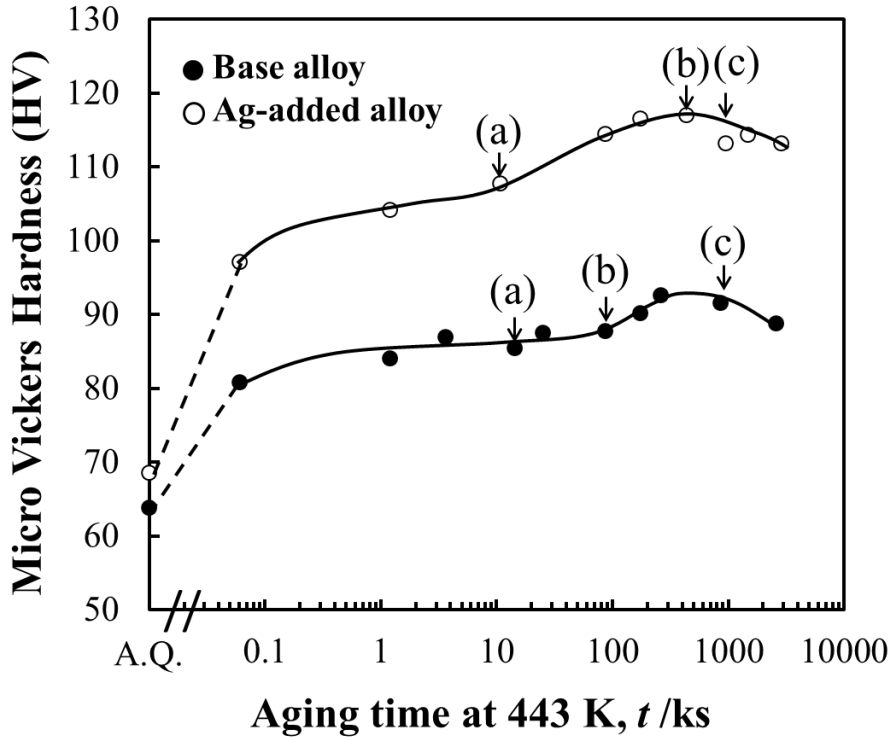

Fig. 1 Hardness curves for the base and Ag-added alloys aged at 443 K. A plateau separates two regions of more rapid hardening. Peak hardness is reached at similar times. TEM microstructures were observed at the aging times indicated by (a), (b) and (c) in Fig. 1.

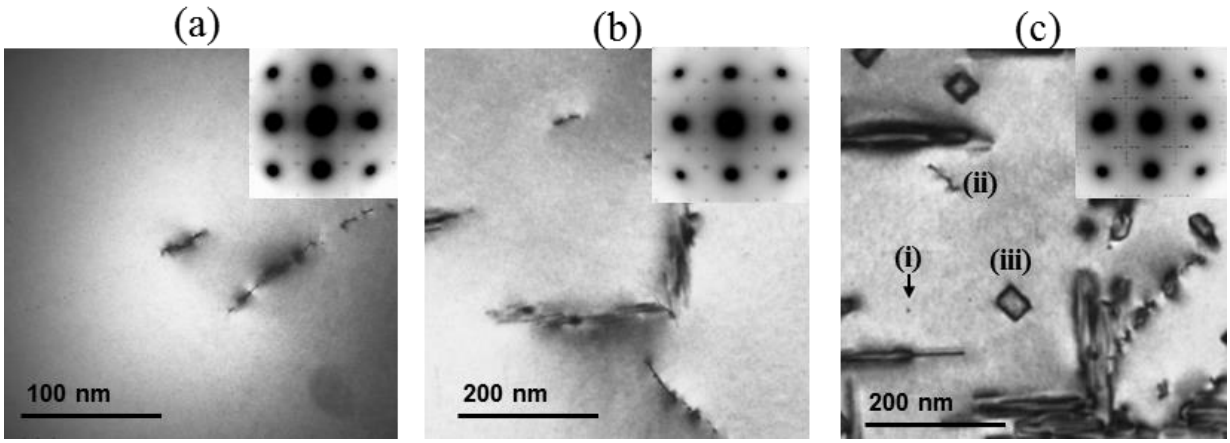

Fig. 2 Bright field TEM images with selected area diffraction patterns taken along $<001>_{Al}$ for the base alloy aged at 443 K for (a) 10.8 ks, (b) 86.4 ks, and (c) 950.4 ks corresponding to the hardness plateau, the second hardening increase, and peak, respectively. Weak fourfold arranged spots in (a-c) show the GPB zones surviving to long ageing times. The typical cross-sections of a GPB zone (i), S' laths (ii), and a Z-phase rod (iii) are shown in (c).

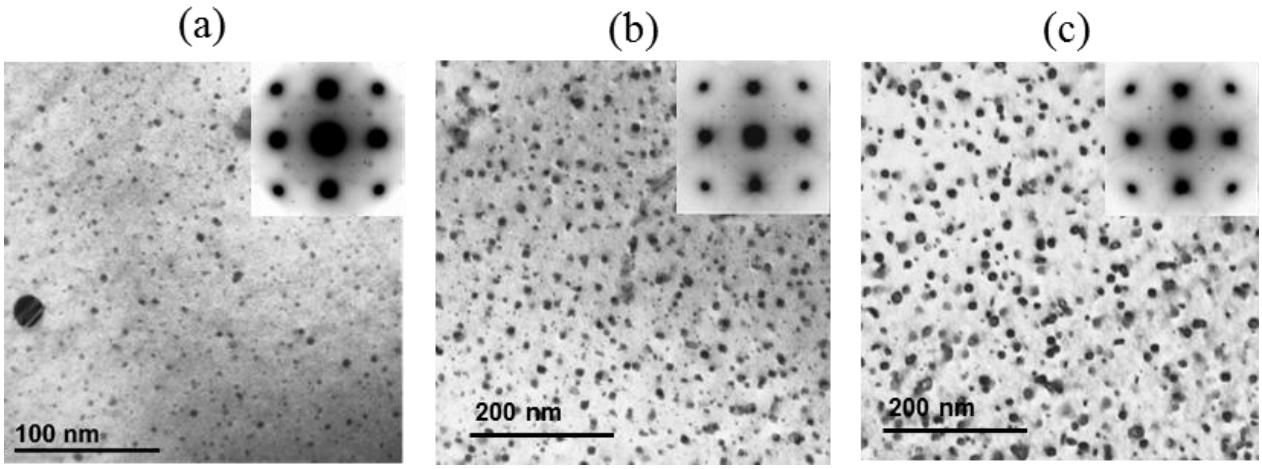

Fig. 3 Bright field TEM images with selected area diffraction patterns taken along $<001>_{Al}$ for the Ag-added alloy aged at 443 K for (a) 10.8 ks, (b) 432 ks, and (c) 950.4 ks.

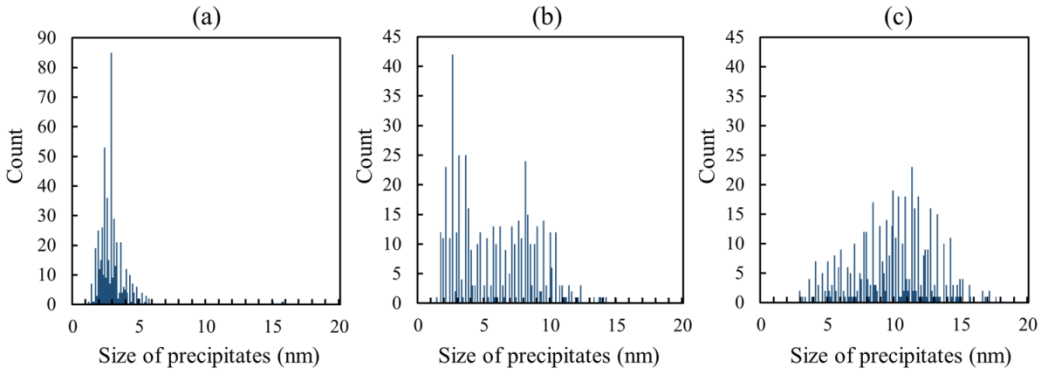

Fig. 4 Size distribution of the precipitates in the Ag-added alloy aged at 443 K for (a) 10.8 ks, (b) 432 ks and (c) 950.4 ks.

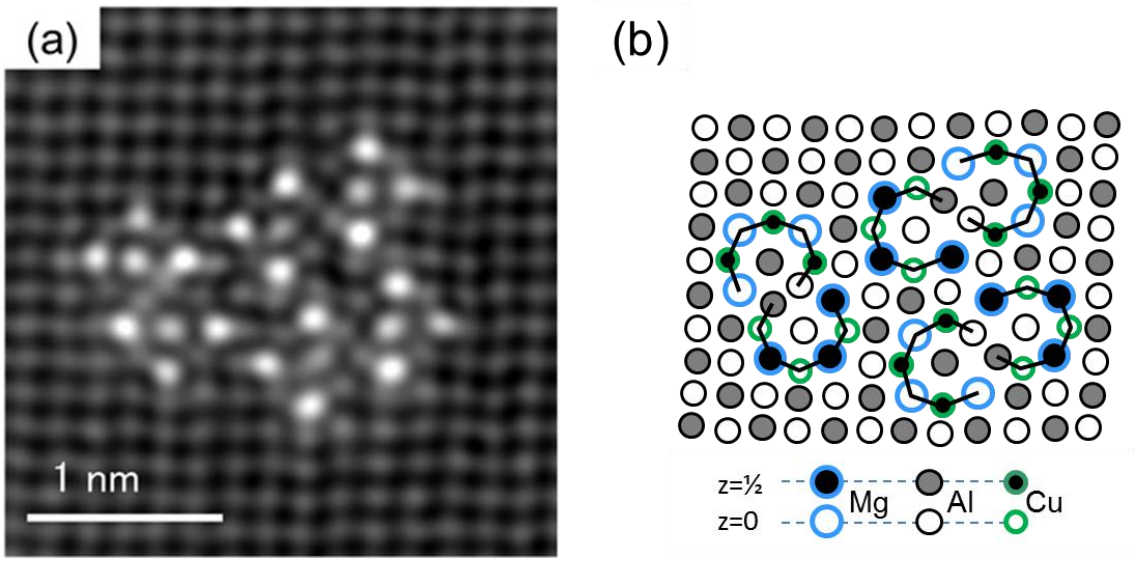

Fig. 5 (a) $<001>_{Al}$ HAADF-STEM image and (b) deduced map of all elemental columns over the cross-section of a GPB zone in the base alloy aged for 950.4 ks (11 days) at 443 K (170 °C). Columns correspond to the two Al planes z=0 and ½ (0.203 nm). Together with the center, a black curve defines the columns of the basic unit ($Al_2Mg_3Cu_3$). Units in a pair are on different heights.

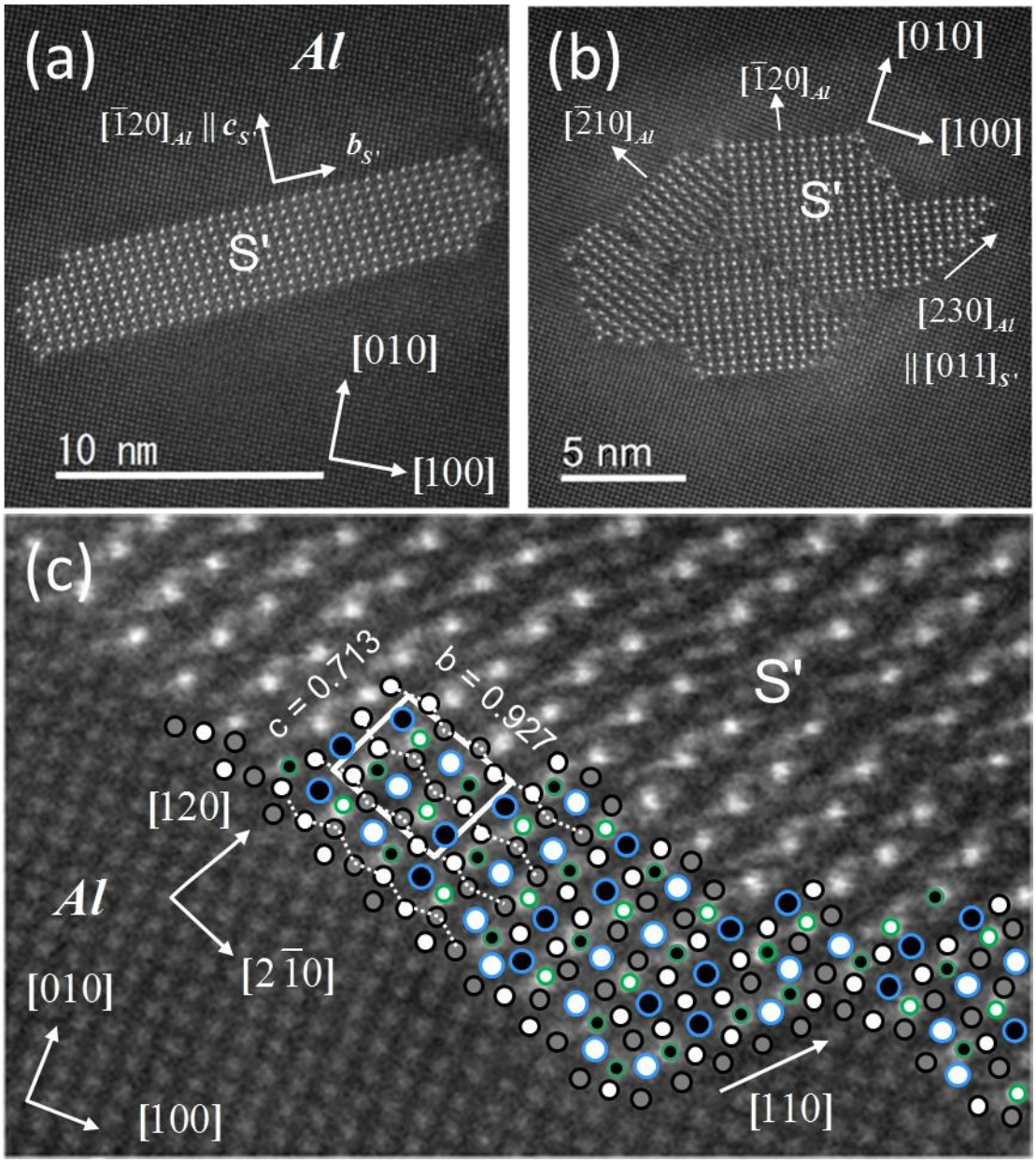

Fig. 6 HAADF-STEM images along <001>Al || [100]S' of S' laths in the Base alloy aged for 950.4 ks at 443 K showing (a) S' main interface has normal $c_{S'} \parallel [1\bar{2}0]_{Al}$, (b) Cluster of laths where $b_{S'}$ and $c_{S'}$ take orthogonal $<120>_{Al}$ directions. Trace of $(230)_{Al} \parallel (011)_{S'}$ interface plane is indicated. (c) Detail of main interface along $b_{S'}$ (and small step along $[100]_{Al}$) with unit cell and superposed map of atoms. The coherent main interface corresponds always with internal Al planes at $z = 0, \frac{1}{2}$ in S' cell (buckled dotted lines). All distances are in nm. See legend in Fig. 5.

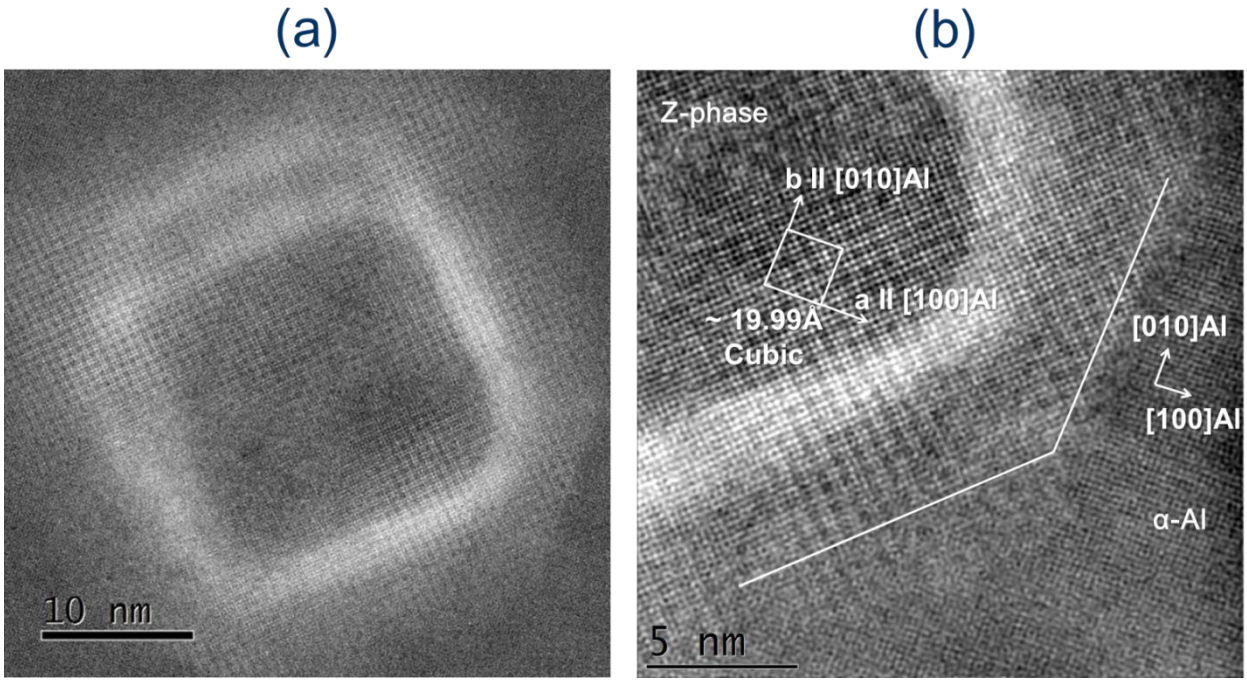

Fig. 7 HAADF-STEM images of the Z phase taken along $<001>_{Al}$ for the base alloy aged for 950.4 ks at 443 K, showing cube on cube orientation relation.

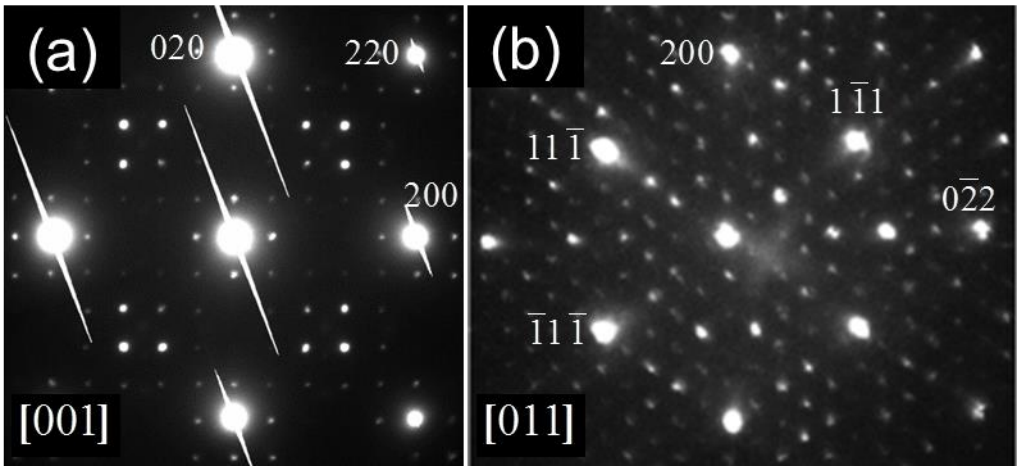

Fig. 8 Nano-beam diffraction patterns of large embedded rod-shaped fcc Z-phase in the Base alloy aged at 443K for 950.4 ks. The Z unit cell is parallel with Al, but 5 times larger: (a) $[001]_{Al,Z}$ projection along a rod, (b) $[110]_{Al,Z}$ projection perpendicular to rod. In (a) the small square of sharp spots (from Z) between Al reflections correspond with the faint spots in the SADP's in Fig. 3(b-c) originating from iQC/T precipitates. Indices for Z are obtained from those of Al by multiplication with 5. Compare with [23].

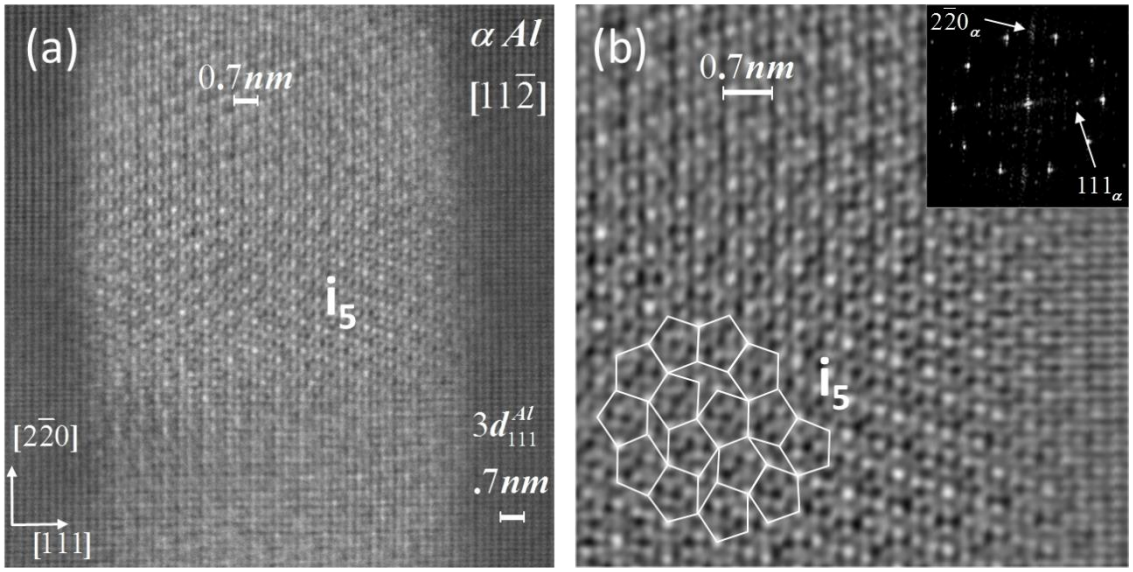

Fig. 9 HAADF-STEM image in a $<112>_{Al}$ zone of a typical precipitate in the Ag-added alloy, here aged at 443 K (170 °C) for 950.4 ks. (a) Region 'i_5' has 5-fold local symmetry. An enlarged magnification is shown in (b). FFT (insert) of i_5 region strongly indicates that Ag addition causes the formation of the icosahedral quasi-crystalline (iQC) precipitates. An overlay with pentagons with vertices on strong spots shows that the 5-fold symmetry has defects.

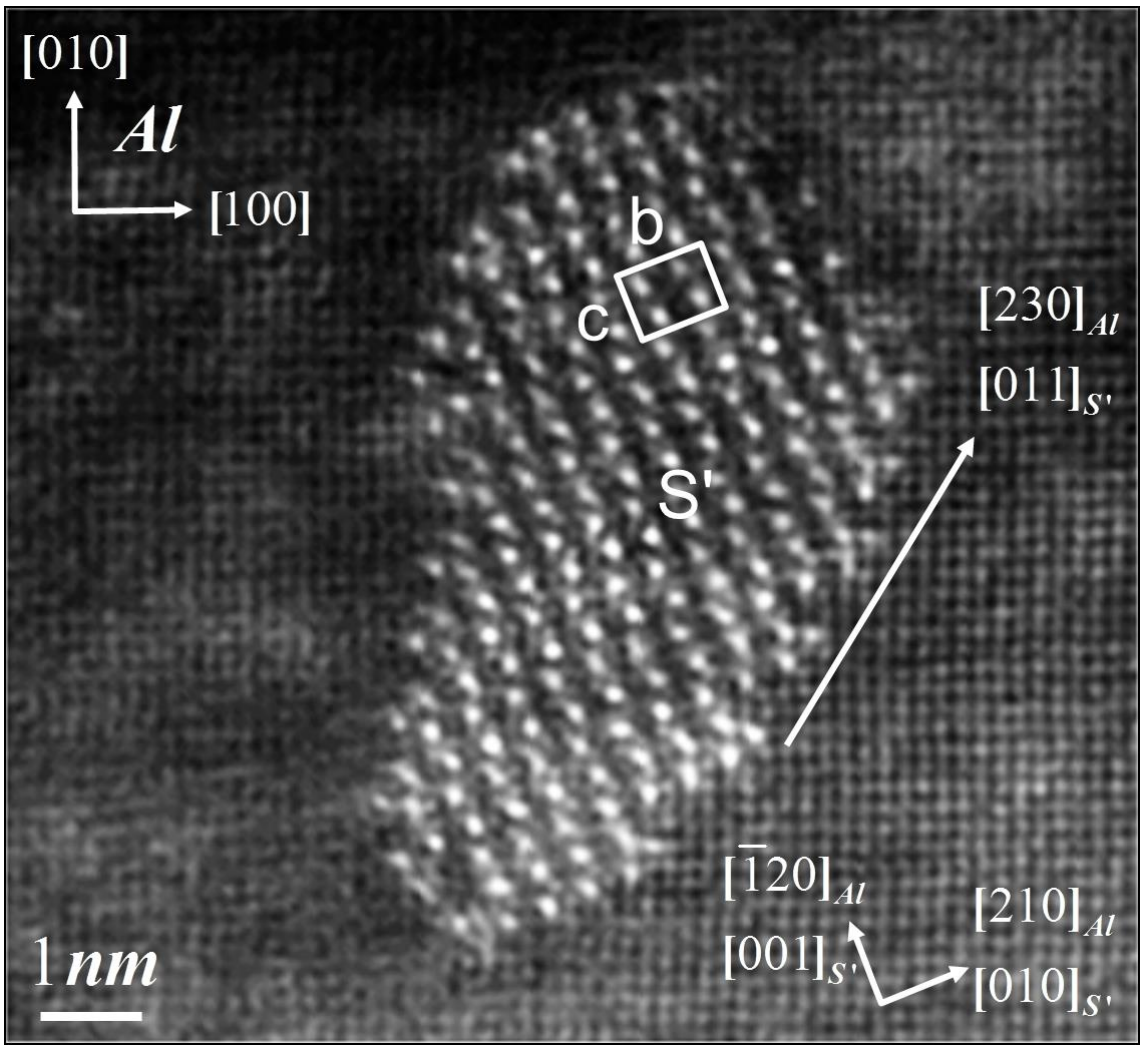

Fig. 10 HAADF-STEM image of the $<100>_{Al}$ zone in the Ag-added alloy aged for 950.4 ks, showing a cross-section of S'- rod (along $[100]_{S'}$). Interface with the trace along $[011]_{S'}$ has higher density of Cu and/or Ag columns. Ag has the effect of refining the particles and giving more roundish cross-sections. The orientation relationship between Al matrix and S' phase is the same as for the base alloy (c.f. Fig. 6).